ACADEMIA ROMÂNĂ
Revue Roumaine de Chimie
https://www.icf.ro/rrch/

Rev. Roum. Chim.,
2024, *69*(10–12), 621–627
DOI: 10.33224/rrch.2024.69.10-12.12

THE STUDY OF PHYSICOCHEMICAL AND ELECTROCHEMICAL PROPERTIES OF NEW HYBRID $PPySO_4$-COATINGS ON Ti6Al4V

Mounira MAIZA, Abderrazak HAMAM* and Abderrahim Hadj LARBI

Research Center in Industrial Technologies CRTI.P.O.Box 64, Cheraga 16014 Algiers, Algeria

Received June 25, 2024

In the present study, the Polypyrrole (PP_ySO_4) thin films are obtained through electropolymerization of pyrrole on Ti6Al4V (TA6V) alloy substrate (PP_ySO_4/ TA6V) by using cyclic voltammetry (CV). Structure, surface morphology and electrochemical properties of the PP_ySO_4/ TA6V thin films were studied by Scanning Electron Microscope (SEM) coupled with energy dispersive X-ray spectrometry (EDX), X-ray diffraction spectroscopy (DRX), Raman spectroscopy (RAMAN), X-ray photoelectron spectroscopy (XPS) and electrochemical impedance spectroscopy (SIE).

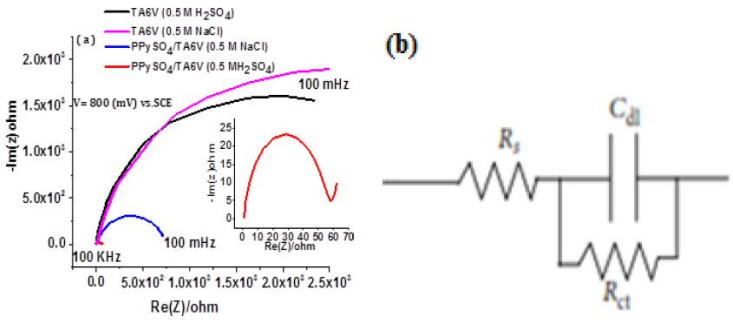

INTRODUCTION

In this study, aim of this work is to synthesize the new hybrid electrode PPySO4 / TA6V by a simple electrochemical polymerization process, it is important that the electrode does not oxidize at the same time as the monomer, is the case with TA6V.[1]

To utilize conductive polymers for electrode modification, strong adhesion between the polymer films and electrode substrates should be ensured with high electrical/electrochemical activities. Electrically conductive polymers, such as polypyrrole (PPy), have been extensively studied as active electrode materials and supporting additives for a number of applications, including electronics, batteries, electrodes, and biomaterials.[2–6] PPy is a widely studied conductive polymer because of its high conductivity, chemical stability, and biocompatibility.[7,8]

In this study, aim of this work is to synthesize the new hybrid electrode $PPySO_4$ / TA6V by a simple electrochemical polymerization process. Polypyrrole deposits easily on TA6V in in the H_2SO_4 solution. The electrochemical polymerization of $PPySO_4$ on TA6V substrate in H_2SO_4 solution (0.5 M) was presented for the first time and improved the electrochemical properties of the TA6V alloy (conductivity). The new hybrid

* Corresponding author: hamam.abderrazak@yahoo.com

electrode $PPySO_4$ / TA6V through a facile fabrication protocol holds great promise for the applications in fuel cell technologies.

MATERIALS AND METHODS

Materials

Pyrrole (> 98% purity, Prolabo product) and Sulfuric acid (Merck product). All aqueous solutions were prepared with bi-distilled water (presenting high resistance ~18MΩ). This procedure was sufficient to obtain reproducible results. In all experiments, TA6V commercial alloy samples (Ti6Al4V) were used as substrates. The geometric surface of the working electrode was equal to 2 cm^2.

Preparation of modified $PPySO_4$/TA6V electrodes

The TA6V electrode (surface of 2 cm^2) was used as the working electrode in one compartment electrochemical cell for PPy deposition. Before the electrochemical experiments and in order to activate the electrode surface, TA6V was firstly immersed for 10 min in the solution containing 2 M hydrochloric acid (HCl) and then rinsed several times with distilled water.[9,10] The second step was deposition of $PPySO_4$ onto the TA6V alloy from the electrochemical plating bath containing pyrrole (0.1M), H_2SO_4 (0.5M). The $PPySO_4$ loading is expressed as electrodeposition cycles voltametry. After being electrodeposited the $PPySO_4$ onto TA6V alloy substrate Scheme 1, the electrode was washed with triply distilled water and subjected to its structure, surface morphology and electrochemical properties characterization.

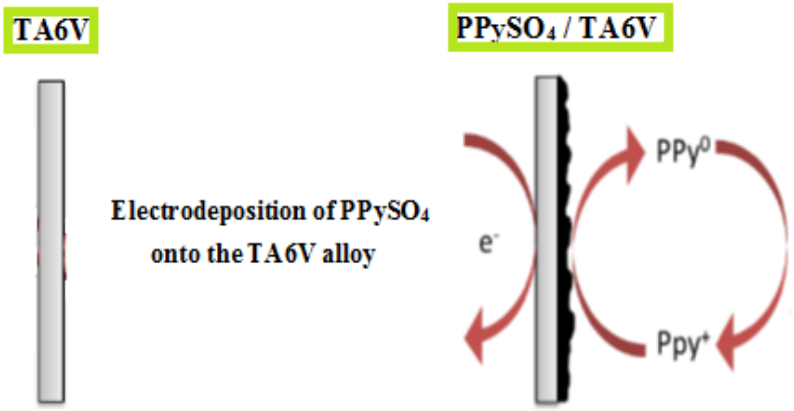

Scheme 1 – Schematic representation of $PPySO_4$ electrodeposition onto TA6V substrate.

Electrochemical measurements

For electrochemical measurements, the experiments were carried out in a conventional three-electrode in one compartment of electrochemical cell for $PPySO_4$ deposition. A saturated calomel electrode (SCE) placed in a separate compartment containing the supporting electrolyte and a platinum wire electrode were used as reference and auxiliary electrode, respectively. The polarization curves, at a scan rate of 20 mV s^{-1} and electrochemical impedance spectroscopy (EIS) tests were carried out in aerated solution using an AUTOLAB Potentiostat/Galvanostat (PGSTAT30) under FRA software. For EIS tests have been measured of an electrochemical system to a.c. excitation with a frequency ranging from 100 kHz to 10 mHz and peak to peak a.c. amplitude of 10 mV. The impedance diagrams are given in the Nyquist representation.

The range of potential used for electropolymerization of PPy by cyclic voltammetry is E = 0.00–1.0 V vs. SCE at scan a rate of v = 20 mV/s (Fig. 1).

Surface analysis

The morphology of the samples was performed by Field Emission Gun-Scanning Electron Microscope (FEG-SEM, ultra 55 Zeiss), coupled with Energy Dispersive X-ray elemental analysis (EDX) which permit the determination of their elemental compositions. During analysis, the sample was glued with conductive cement on a stub. The Si/Li electrode was used for light elements with a 133eV resolution at low rate counting with beam parameters of 20 keV and 160 pAm. The EDX

collector time was 100s. In addition to these measurements, XRD (X-ray diffraction) was also used. XP spectra were recorded using a K Alpha (Thermo) a monochromatic Al Kα X-ray source (hα =1486.6 eV, spot size: 400 µm). The pass energy was set to 200 and 50 eV for the survey and the narrow regions, respectively. Electron and argon flood guns were used to compensate for the static charge built up on the film surface. The composition was determined using the manufacturer's sensitivity factors.

RESULTS AND DISCUSSION

Electrochemical preparation of the modified PP_ySO_4/ TA6V electrode

Figure 1a, b show cyclic voltammograms recorded on TA6V substrate during the first and 20 continuous cycles, respectively. The potential was varied between 0.00 and 1 V vs. SCE at a scan rate of 20 mV/s. Figure 1a are presented the electropolymerization of pyrrole at the TA6V electrode with and without 0.1 M pyrrole. Without pyrrole, the anodic reaction rate is low and remains low over the entire potential range covered (Fig. 1a). But in the presence of pyrrole an anodic peak is observed at around 0.8 V. This peak is characteristic au first oxidation of pyrrole monomer, which are responsible for the growth of the PP_ySO_4 film on the surface of the TA6V (Fig. 1a). In Fig. 1b, as the number of cycles increased, new oxidation picks had gradually appeared, suggesting a progressive increase in the deposition rate of the PP_ySO_4 onto the TA6V surface. The oxidation of pyrrole onto TA6V substrate followed by a black deposit of PPy covering the whole electrode surface.

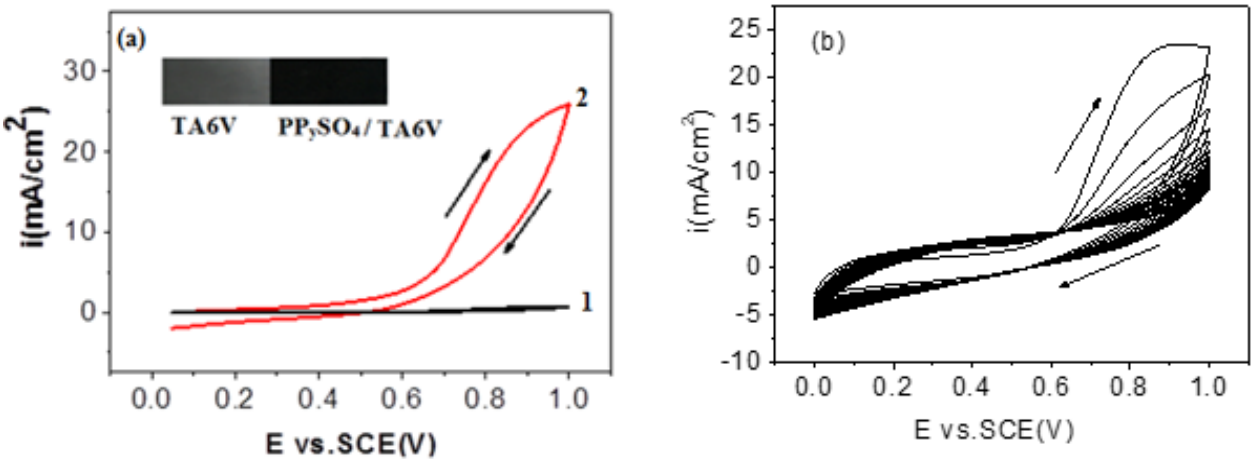

Fig. 1 – Cyclic voltammograms of electropolymerization of pyrrole on TA6V electrode: a**)** first cycle ((1) TA6V electrode (0 M pyrrole), (2) TA6V (0.1 M pyrrole)); b) 20 continuous cycles. Obtained in 0.5 M H_2SO_4 solution at 20 mV s^{-1} and T 25 °C.

Scanning Electron Microscope coupled with energy dispersive X-ray spectrometry

The SEM images of the polypyrrole thin film deposited on the TA6V substrate shows that the morphologies obtained on the surface of the thin film after electrochemical polymerization, consisting of spherical particles gathered in the form of cauliflower[11–13] (Fig. 2b), which completely cover the network of TA6V substrate with a uniform, smooth and homogeneous film.

The EDX spectrum of the $PPySO_4$ / TA6V hybrid thin film in Fig. 2d shows the presence of the main elements of PPy namely carbon and nitrogen, oxygen, the components of TA6V alloy and the element sulfur which represents a constituent of the H_2SO_4 synthesis solution.

The polypyrrole thin film is strongly adherent and remains attached to the surface even after several washes.

Figure 2c illustrates the EDX spectrum relating to the TA6V nu substrate. The analysis shows the presence of peaks relating to the different compositional elements of TA6V, namely aluminum, titanium and vanadium.

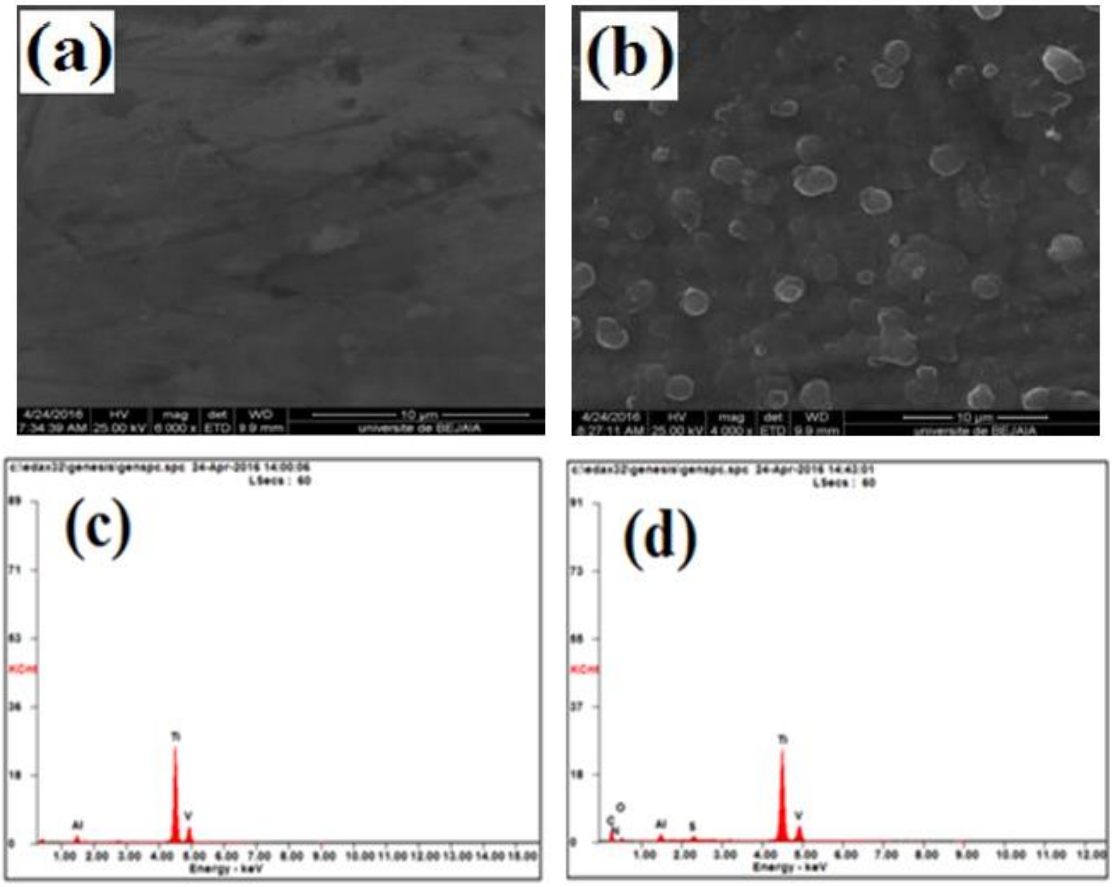

Fig. 2 – a) SEM images of TA6V; b) $PPySO_4$-coated TA6V (10 um); c) corresponding EDX mapping profiles for the TA6V; d) $PPySO_4$-coated TA6V. Obtained with synthesis conditions: concentration of monomer (pyrrole) 0.1 M, 0.5 M H_2SO_4, scan rate of 20 mV s–1 and T = 25°C.

Surface analysis by XPS

Figure 3 displays the survey and N1s narrow regions of the electro synthesized $PPySO_4$ film on TA6V alloy substrate. The survey region (Fig. 3a) exhibits S2p (168.7 eV), C1s (285), N1s (399.9 eV) and O1s (532.2 eV). The peak positions of the S2p and O1s core levels are close to the previously reported values of 168.6 eV and 532.1 eV respectively,[14,15] for Na_2SO_4. The N1s region (Fig. 3b) is fitted with four components centered at 398.4,399.9, 401.0, and 402.3 eV assigned to C=N defects, N H, and two positively charged types of nitrogen atoms, noted N^+(I) and N^+(II).

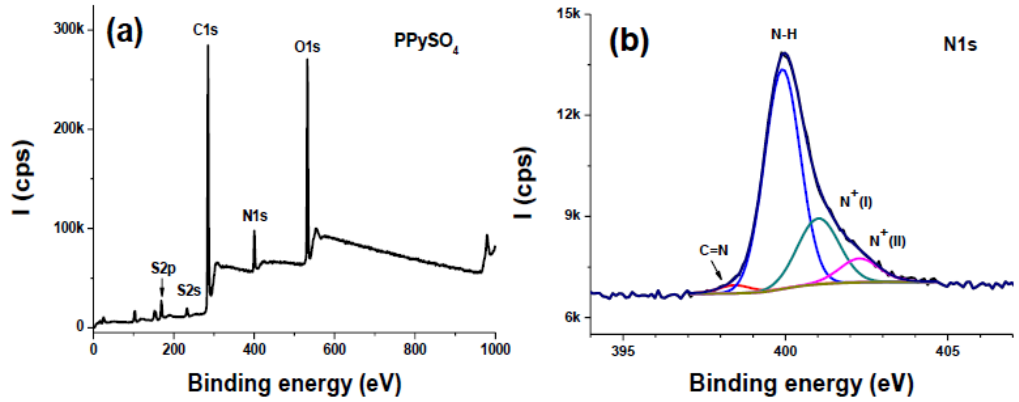

Fig. 3 – Survey (a) and high resolution N1s (b) regions of $PPySO_4$ film electro synthesized on TA6V alloy electrode.

Table 1

Reports the surface composition of the $PPySO_4$ film by considering the atomic ratios of C, O and S and the various chemical states of nitrogen.

Materials	C	N(C=N)	N(N-H)	N^+(I)	N^+(II)	S	O
Corelevel BE (eV)	284.8	398.4	399.9	401.0	402.3	168.7	532.2
Atomic percent	68.2	0.17	3.88	1.34	0.48	2.71	23.2

The C/N ratio is 11.6, higher than the theoretical ratio of 4, probably due to adventitious hydrocarbon contamination, since polypyrrole is a high surface energy material[16] and is thus expected to get readily contaminated.

The doping level can be calculated using the S/N atomic ratio or the positively charged nitrogen atom contribution to the whole N content $[(N^+(I)+N^+(II))/N]$. These ratios yield 46.2 % and 31.0 %, respectively. Al though these values are not matching, they indicate never the less a high doping level of the polypyrrole film prepared in the experimental conditions described above.

Finally, the O/S ratio is higher than 4, probably due to surface contamination and oxidation of the polymer chain.

X-ray diffractometry (XRD) and Raman spectroscopy

Figure 4 (a). Shows the diffraction spectrum of X-rays at room temperature of modified thin film ($PPySO_4$ / TA6V). The DRX diagram records a broad diffraction peak at $2\theta \sim 27$ ° which attributed to Ppy.[17] For the other diffraction peaks, they are associated with the TA6V alloy substrate.[18]

The Raman analysis before and after synthesized new hybrid electrode PP_ySO_4-coated TA6V alloy (Fig. 4(b)) was carried out to further confirm the presence of active materials. A few broad peaks at 1583 cm^{-1} (C=C stretching), 1373 cm^{-1} (C-N stretching), 1085 cm^{-1} and 928 cm^{-1} (C-H ring deformation vibration) are associated to the characteristics of PPy.[19,20]

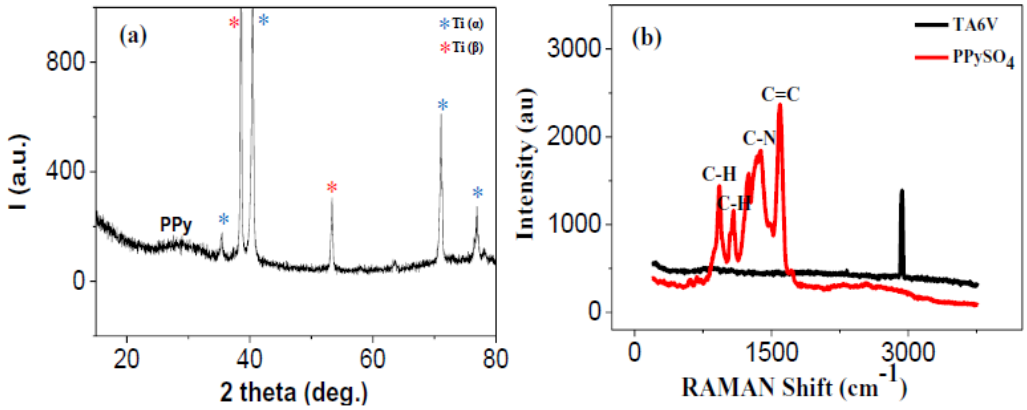

Fig. 4 – a) XRD patterns of PP_ySO_4/TA6V synthesis by voltammetry cyclic; b) Raman spectra of TA6V and $PPySO_4$/TA6V films electrochemically deposited.

Impedance studies

Figure 5 displays a comparison of the TA6V and $PPySO_4$ impedance in 0.5 M of H_2SO_4 and 0.5 M NaCl at 800 mV (vs. SCE), which demonstrates would expect-noticeable differences in impedance before and after oxidation of pyrrole. The decreasing charge transfer resistance before and after oxidation of pyrrole indicates an excellent structural stability and conductivity of $PPySO_4$ electrode. However, the electrolyte (0.5 M H_2SO_4, 0.5 M NaCl) impedance it plays an important and special role in conductivity of $PPySO_4$ which be attributed to conductivity of electrolyte, as the low impedance and high conductivities are important requirements for various applications, including pressure monitoring,[21,22] temperature sensing[23,24] and strain gauges.[25,26] Moreover, high-conductivity electrodes are important in energy conversion devices like batteries,[27,28] fuel cells,[29,30] and electrolyzers,[31,32] where they facilitate chemical reactions and efficient conversion between electrical and chemical energy, thereby enhancing device performance.[33]

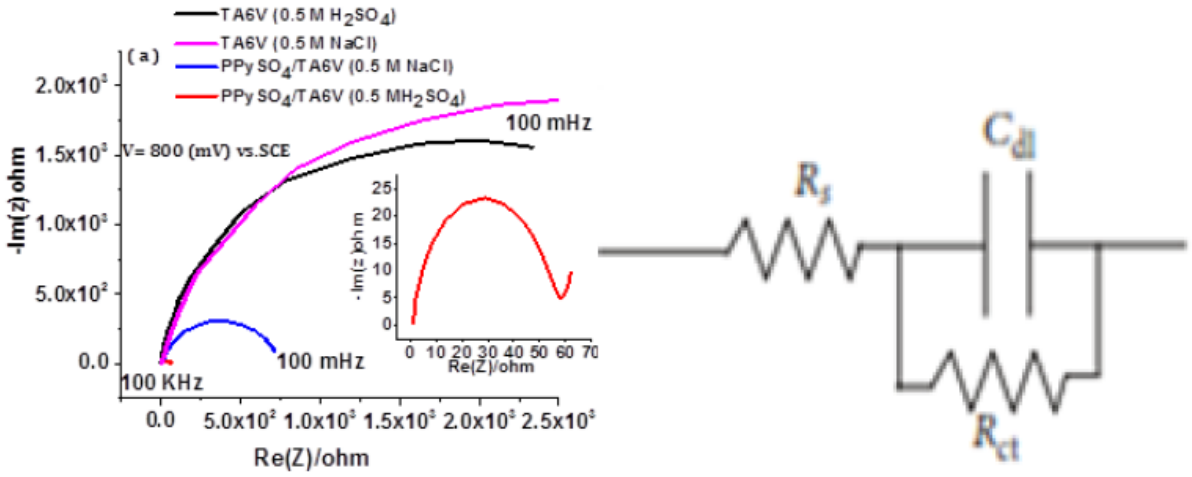

a) b)

Fig. 5 – a) Impedance spectra of TA6V and $PPySO_4$/TA6V electrode; b) Equivalent circuit used for analysis of data obtained from PPy films.

These curves are depressed in nature with their center below the x-axis. By using Setup - ZSimDemo-320 program, the impedance diagrams can be fitted by a simple equivalent circuit (insert of Fig. 5b) composed by R_s (solution resistance), R_{ct} (charge transfer resistance) and CPE (constant phase element of double layer capacitance (C_{dl})). The C_{dl} was estimated from the impedance value of the frequency (f_m) having maximum imaginary component with Nyquist plot by using the following relationship:

$$C_{dl} = 1/2\pi f_m R_{ct} \quad (1)$$

The charge-transfer resistance (R_{ct}) values used in Eq. (1) were given by the Setup- ZSimDemo-320 program by fitting the Nyquist plots.

CONCLUSION

The present work is devoted to the preparation of new hybrid obtained onto TA6V substrate by simple electrochemical polymerization process. The morphologies of the $PPySO_4$ after electrochemical polymerization, consisting of spherical particles gathered in the form of cauliflower, which completely cover the network of TA6V alloy substrate with a uniform and homogeneous film. The $PPySO_4$ thin film is strongly adherent. It can also be concluded that polypyrrole has improved the electrochemical properties of the TA6V alloy. The new hybrid electrode PPySO4 / TA6V foam electrode through a facile fabrication protocol holds great promise for the applications in fuel cell technologies.

Acknowledgements. The authors wish to acknowledge the Algerian Ministry of Higher Education and Scientific Research for supporting this work.

REFERENCES

1. 1.R. Siab, G. Bonnet, J. M. Brossard, J. F. Dinhut, *Appl. Surf. Sci*., **2004**, *236*, 50–56; https://doi.org/ 10.1016/ j.apsusc.2004.03.258
2. 2. L. Jin, P. Wang and Z. Song. *Sci. Rep*., 2016, *6*, 32919; https://doi.org/10.1038/srep32919
3. 3. C. B. Bufon and T. Heinzel, *Appl. Phys. Lett*., **2006**, *89*, 012104; https://doi.org/10.1063/1.2219375
4. 4. N. K. Guimard, N. Gomez and C. E Schmidt, *Prog. Polym. Sci*., **2007**, *32*, 876–921; https://doi.org/10.1016/ j.progpolymsci.2007.05.012
5. 5. G. G Wallace, M. J. Higgins, S. E. Moulton and C. Wang, *Nanoscale*, **2012,** *4*, 4327–4347; https://doi.org/ 10.1039/c2nr30758h
6. 6. A. Guiseppi-Elie, **2010,** *31*, 2701–2716; https://doi.org/ 10.1016/j.biomaterials.2009.12.052
7. 7. G. Cooper, R. Noufi, A. J. Frank and A. J. Nozik, *Nature*, **1982**, *295*, 578–580; https://doi.org/10.1038/ 295578a0
8. 8. A. Ramanavičius, A. Ramanavičienė and A. Malinauskas, *Electrochim. Acta*, **2006**, *51*, 6025–6037; https://doi.org/10.1016/j.electacta.2005.11.052
9. 9. A. Hamam, C. Dehchar, M. Maiza, I. Chikouche and H. Merabti, *Int. J. Electrochem. Sci*., **2020**, *15*, 3534 –3542; https://doi.org/10.20964/2020.04.15
10. 10. A. Hamam and M. Maiza, *Int. J. Electrochem. Sci*., **2021**, *16*, 210426; https://doi.org/10.20964/2021.04.37
11. 11. A. Hamam, D. Oukil, A. Dib, H. Hammache, L. Makhloufi and B. Saidani, *Surf. Rev. Lett*., **2015**, *22*, 1550065; https://doi.org/10.1142/S0218625X15500651
12. 12. A. Hamam, M. Maiza, M. M. Chehimi and D. Oukil, *Cellulose*, **2022**, *29*, 4579–4588; https://doi.org/ 10.1007/s10570-022-04536-3

13. 13. A. Hamam and M. Maiza, *J. Environ. Anal. Chem*., **2022**, *102*, 5185–5193; https://doi.org/10.1080/03067319.2022.2118588
14. 14. R. V. Siriwardane and J. M. Cook, *J. Colloid Interface Sci*., **1986**, *114*, 525; https://doi.org/10.1016/0021-9797(86)90438-8
15. 15. B. J. Lindberg, K. Hamrin, G. Johansson, U. Gelius, A. Fahlmann, C. Nordling and K. Siegbahn, *Phys. Scripta*, **1970**, *1*, 286; https://doi.org/10.1088/0031-8949/1/5-6/020
16. 16. K. Boukerma, M. Mičušík, M. Mravčáková, M. Omastová, M.-J. Vaulay, P. Beaunier and M. M. Chehimi, *Colloids Surf. A Phys. Chem. Eng. Asp*., **2007**, *293*, 28–38; https://doi.org/10.1016/j.colsurfa.2006.07.005
17. M. R. Mahmoudian, Y. Alias, W. J. Basirun and M. Ebadi, *Appl. Surf. Sci*., **2013**, *268*, 302–311; https://doi.org/10.1016/j.apsusc.2012.12.082
18. 18. M. Laveissière, H. Cerda, J. Roche, L. Cassayre and L. Arurault, *Surf. Coat. Technol*., **2019**, *361*, 50–62; https://doi.org/10.1016/j.surfcoat.2018.12.122
19. 19. X. Fan, Z. Yang and N. He, *RSV Adv.*, **2015,** *5*, 15096–15102; https://doi.org/10.1039/C4RA15258A
20. H. Du, Y. Xie, C. Xia, W. Wang and F. Tian, *New J. Chem*., **2014**, *38*, 1284; https://doi.org/10.1039/c3nj01286g
21. 21. M. Vahdani, S. Mirjalali, M. Razbin, S. A. Moshizi, D. Payne, J. Kim, S. Huang, M. Asadnia, S. Peng and S. Wu, *Adv. Sustain Syst*., **2024,** 1–16; https://doi.org/10.1002/adsu.202300482
22. C. Y. Huang, G. Yang, P. Huang, J. M. Hu, Z. H. Tang, Y. Q. Li and S. Y. Fu, *ACS Appl. Mater. Interfaces*, **2023,** *15*, 3476–3485; https://doi.org/10.1021/acsami.2c19465
23. Y. Yu, S. Peng, P. Blanloeuil, S. Wu and C. H. Wang, *ACS Appl. Mater. Interfaces*, **2020,** *12*, 36578–36588; https://doi.org/10.1021/acsami.0c07649
24. H. Xiao, S. Li, Z. He, Y. Wu, Z. Gao, C. Hu, S. Hu, S. Wang, C. Liu, J. Shang, M. Liao, D. Makarov, Y. Liu and R. W. Li, *Adv. Funct. Mater*., 2023, *33*, 1–13; https://doi.org/10.1002/adfm.202214907
25. B. Ketelsen, H. Schlicke, V. R. Schulze, S. C. Bittinger, S. Da Wu, S. hui Hsu and T. Vossmeyer, *Adv. Funct. Mater*., **2023**, *33*, 2210065; https://doi.org/10.1002/adfm.202210065
26. J. Huang, A. Chen, S. Han, Q. Wu, J. Zhu, J. Zhang, Y. Chen, J. Liu and L. Guan, *Adv. Sci*., **2023,** *10*, 1–13; https://doi.org/10.1002/advs.202301116
27. T. H. Chen, S. K. Tsai, J. Y. Chang, E. Chung and C. H. Hou, *Desalination*, **2023,** *558*, 116616; https://doi.org/10.1016/j.desal.2023.116616
28. J. Sang, X. Zhang, K. Liu, G. Cao, R. Guo, S. Zhang, Z. Wu, Y. Zhang, R. Hou, Y. Shen and G. Shao, *Adv. Funct. Mater*., **2023,** *33*, 1–13; https://doi.org/10.1002/adfm.202211640
29. F. Ning, Z. Chai, X. Dan, P. Liu, Q. Wen, S. Pan, C. He, Y. Li, H. Jin, W. Li, P. Xu, J. Chen, J. Wei and X. Zhou, *Small Methods*, **2023,** *7*, 1–12; https://doi.org/10.1002/smtd.202201256
30. Z. Li, L. Gao, J. Liu, W. Chen, X. Li, X. Wu, X. Jiang, G. He and X. Yan, *J. Memb. Sci*., **2024,** *700*, 122673; https://doi.org/10.1016/j.memsci.2024.122673
31. J. Zhang, J. Pan, Y. Yuan, Q. Zhang, P. Fang, H. Zhang, Q. Yu, T. Zhou, Z. Sun and F. Yan, *Chem. Mater*., **2024**, *36*, 5720–5729; https://doi.org/10.1021/acs.chemmater.4c00787
32. D. Aili, M. R. Kraglund, S. C. Rajappan, D. Serhiichuk, Y. Xia, V. Deimede, J. Kallitsis, C. Bae, P. Jannasch, D. Henkensmeier and J. O. Jensen, *ACS Energy Lett*., **2023,** *8*, 1900–1910; https://doi.org/ 10.1021/acsenergylett.3c00185
33. Y. Chu, Z. Sha, S. A. Brown, S. He, S. Wu, C. H. Wang and S. Peng, *Adv. Nanocomp*., **2024,** *1*, 275–289; https://doi.org/10.1016/j.adna.2024.08.001